SRTTU

JCARME
ISSN: 2228-7922
Journal of Computational and Applied Research in Mechanical Engineering
Vol. 9, No. 1, pp. 57-72
jcarme.sru.ac.ir

Crashworthiness design of multi-cell tapered tubes using response surface methodology

S. Pirmohammad[a,*], S. Esmaeili-Marzdashti[a] and A. Eyvazian[b]

[a] *Mechanical Engineering Department, Faculty of Engineering, University of Mohaghegh Ardabili, P.O. Box 179, Ardabil, Iran*
[b] *Mechanical and Industrial Engineering Department, College of Engineering, Qatar University, P.O. Box 2713, Doha, Qatar*

Article info:
Received: 16/08/2017
Accepted: 01/11/2018
Online: 04/11/2018

Keywords:
Crashworthiness,
Axial and oblique dynamic loading,
Response surface methodology,
TOPSIS.

Abstract
In this article, crashworthiness performance and crushing behavior of tapered structures with four internal reinforcing plates under axial and oblique dynamic loadings is investigated. These structures have a tapered form with five cross-sections of square, hexagonal, octagonal, decagon and circular shapes. In the first step, finite element simulations performed in LS-DYNA are validated by comparing with experimental data. The code generated in LS-DYNA is then used to investigate the energy absorption behavior of the tapered structures. Response surface methodology and historical data design technique are employed to optimize the cross section perimeter (or tapered angle) of the tapered structures by considering two conflicting crashworthiness criteria including energy absorptionand peak crushing force. The optimization results show that the optimal tapered angle is enhanced by increasing the number of cross-section sides (or the number of corners). Then, the optimized tapered structures with different cross-sections are compared with each other using a ranking method called TOPSIS to introduce the most efficient energy absorber. The decagonal structure is finally found to be the best energy absorber.

Nomenclature

a	Side length	m	Number of criteria
A^+	Positive ideal solution	P	Perimeter
A^-	Negative ideal solution	$\overline{F}$	Peak crushing force
A_{ij}	Decision matrix	R	Radius of circular structure
C_i^+	Proximity coefficient of each option		Normalized decision matrix
DOE	Design of experiment	S_i^-	Distance of the negative ideal
$D_{1\text{-}5}$	Optimal points	S_i^+	Distance of the positive ideal
E	Young's modulus	t	Wall thicknesses
EA	Energy absorption		

[*] *Corresponding author*
email address: s_pirmohammad@uma.ac.ir

vij	Weighted normalized decision matrix
v	Velocity
w	Weight
wi	Relevant weight
Θ	Tapered angle
σ_{ut}	Ultimate stress
σ_y	Yield stress
$F(x)$	Variations of crushing force
Y	Poisson variation
Δ	Total displacement

1. Introduction

Collision data gathered by different researchers [1-3] show that although older car occupants involved in car collisions are likely less than younger occupants, older occupants are more likely killed in the car crash events. On the other hand, the number of older car users increases implying that safety in cars must be further improved.

Crashworthiness is the term used to define the capacity of structures to protect a vehicle occupant during a crash. Crashworthiness of structures is a branch of impact mechanics specifying the reaction of the structures to reduce the damage when a crash occurs. This field of research has applications in automotive, rail, aviation and aerospace industries. Crashworthy structures dissipate the kinetic energy by elastic-plastic deformations during the crushing process. By increasing the safety requirements in the transportation system and issues related to the crashworthiness performance of structures, a set of basic researches have been conducted on energyabsorbing structures with different cross-sections and materials. These studies are a set of numerical and experimental researches on different cross-sections. These cross-sections have circular [4-7], polygonal, quadrangular and rectangular shapes [8-10]. The use of crashworthy structures with high energy absorption capacity and desirable deformation is very common. Moreover, there exist several types of research focused on the improvement of energy absorption performance of the thin-walled structures by using fillers such as metallic [11-14] and polymeric foam [15, 16].

Majority of the previous investigations have been focused on crashworthiness of single-cell tubes. For example, Abramowicz and Jones [17, 18] investigated the crashworthiness of steel square tubes. They observed symmetric and asymmetric folding mechanisms in the crushing process. Langseth and Hopperstad [19] studied the collapse behavior of square and circular tubes under dynamic and static loads. They concluded that the average crushing force in static loading is greater than that in dynamic loading. Also, they observed the same crushing mechanism in the square and circular cross-sections. Hosseini-Tehrani and Pirmohammad [20] investigated the energy absorption capacity of polygonal straight structures under axial and oblique loadings. They observed that the structure with the octagonal cross-section has a great potential to absorb crash energy. Eivazian [21] and Eyvazian et al. [22, 23] theoretically, numerically and experimentally investigated crash behavior of the corrugated tubes. Their results show that these tubes have desirable energy absorption characteristics.

Multi-cell thin-walled tubes have been proven to have an acceptable energy absorption capacity considering their weight [24]. From the numerical task performed by Zhang and Cheng [25], it is concluded that the energy absorption efficiency in multi-cell tubes is about 50 to 100 percent more than the tubes filled by foam. Qiu et al. [26] investigated the collapse behavior of the single-cell and multi-cell straight tubes with a hexagonal cross-section. They concluded that the multi-cell tubes are more efficient than single-cell ones. Pirmohammad and Esmaeili-Marzdashti [27, 28] have recently proposed multi-cell tubes with a new design of cross-sectional profiles to improve the crashworthiness capacity.

Several studies can also be found in the literature on the tapered tubes. For example, Chang et al. [29] studied the energy absorption and crushing behavior of simple and multi-cell tapered tubes with a square cross-section under dynamic loading. They found that the multi-cell tapered tubes has better energy absorption performance than simple ones. They also found that the energy absorption is improved by increasing the cone angle. In another study, Hosseini-Tehrani

and Pirmohammad [30] studied crashworthiness of the tapered structure with a rectangular cross-section under multiple dynamic loading. They optimized dimensions of this structure and observed that the tapered tubes perform very well in comparison with straight tubes. In another study, Hanfeng et al. [31] studied crashworthiness of the foam-filled tapered tubes with a circular cross-section. They found that the presence of foam plays an important role in increasing the strength to enhance energy absorption capacity. Ahmad and Thambiratnam [32, 33] investigated crashworthiness of circular tapered columns subjected to quasi-static and dynamic axial loadings. Ahmad et al. [34] assessed the crushing capacity of foam-filled tapered columns. In another study, Ghamarian et al. [35] investigated crashworthiness of circular end-capped tapered columns experimentally and numerically. Furthermore, several types of research can be found on the crashworthiness of tapered square columns [34, 35].

The current study investigates the energy absorption behavior of tapered structures, with square, hexagonal, octagonal, decagon and circular cross-sections, reinforced with four internal plates under axial and oblique dynamic loadings. The tapered angle of these structures is optimized by response surface (RS) methodology and historical data design (HDD) technique.

2. Geometry of the sectional configurations

In this study, the collapse behavior of the tapered structures is evaluated. Fig. 1 shows these multi-cell tapered structures having square, hexagonal, octagonal, decagon and circular cross-sections. Four reinforcing plates are used in these structures. The parameter a in all the cross-sections refers to the side length (but in the circular structure, a refers to the diameter). The cross-sectional perimeter of all the tapered structures at the large end is assumed the same and is equal to 320 mm, while it is varied between 20 mm and 320 mm at the small end for the optimization purposes. In order to keep the weight constant, the structures are assigned with different wall thicknesses. In addition, the total length of the structures is taken the same and is equal to 310 mm.

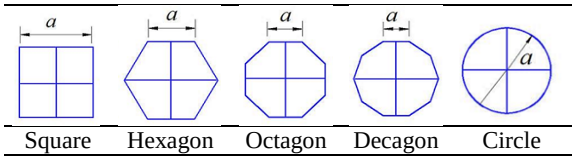

Fig. 1. Sectional configurations of the tapered structures.

3. Finite element modeling

Non-linear explicit finite element code LS-DYNA is employed to simulate the collapse behavior of the tapered structures depicted in Fig. 1. Boundary and impact conditions used in the simulations are seen in Fig. 2. The large end of the tapered structures is fully fixed in all directions, while the small end is assumed free. As is seen in Fig. 2, a rigid-wall, modeled by MAT-RIGID material having the velocity of 15 m/s and weight of 600 kg, crushes the tapered structures with the amount of 225 mm (over 70% of the total length) under axial and different oblique loadings α=0°, 10°, 20° and 30°. Aluminum alloy AA6060-T4 is used as the material of these structures because of having greater strength to weight ratio in comparison to steel. The mechanical properties of this alloy are: σ_y=80MPa, σ_{ut}=173MPa, E=68.2GPa, ρ=2700 kg/m^3, and υ=0.33. Variations of the stress versus strain in the plastic zone are presented in Table 1. To consider the strain hardening effects in the simulations, the energy equivalent flow stress is calculated from the following equation:

$$\sigma_o = \sqrt{\frac{\sigma_y \sigma_{ut}}{1+m}} \tag{1}$$

where, m is the strain hardening exponent of AA6060-T4, which is equal to 0.23. The flow stress is calculated 106 MPa for AA6060-T4 using the abovementioned parameters. It is worth mentioning that the strain rate effect is neglected in finite element analyses because the alloy is insensitive to the strain rate [36].

The structures are modeled in LS-DYNA using the Belytschko-Lin-Tsay quadrilateral shell

formulation with five integration points through the thickness. In order to determine an appropriate element size in meshing the structures, a convergence analysis is performed, and the element size is eventually found as 2 mm × 2 mm. The contact between the rigid-wall and the tapered structures is defined by AUTOMATIC-SURFACE-TO-SURFACE algorithm. Furthermore, the AUTOMATIC-SINGLE-SURFACE algorithm is used to avoid the tube walls penetrating into each other, and Coulomb friction is taken 0.15 for all the structures considered in this research [37]. The material code called 24, MODIFIED-PIECEWISE-LINEAR-PLASTICITY, is utilized to model the AA6060-T4 properties in LS-DYNA.

Table 1. Variations of the stress vs strain in the plastic zone

Strain	0	0.005	0.02	0.06	0.1	0.15	0.18
Stress (MPa)	80	82	113	143	160	166	173

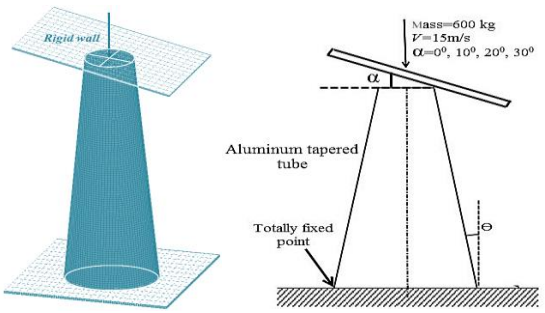

Fig. 2. Computational models for axial dynamic loading

4. Validation of numerical analyses

Extruded circular tubes of radius 25 mm, thickness 1 mm and length 100 mm are experimentally tested under axial dynamic loading. These specimens are tested using a free fall drop hammer, while the hammer weight and height are 59 kg and 1.4 m, respectively. In addition, the speed of the hammer at the moment of impact on the tubes is 8 m/s (see Fig. 3).
Results of the experiments, namely deformation modes, and force-displacement curves, are presented in Fig. 4. Crush behavior of the specimens tested by hammer drop apparatus is simulated in LS-DYNA, as well. The numerical results are given in Fig. 4 for comparison with the experimental results. The figureshows good consistency between the numerical and experimental results. Therefore, the finite element model generated in LS-DYNA can correctly predict the collapse behavior of the tubes, i.e., both the collapse mode and the force-displacement curve.

Fig. 3. Schematic of the free-fall drop hammer.

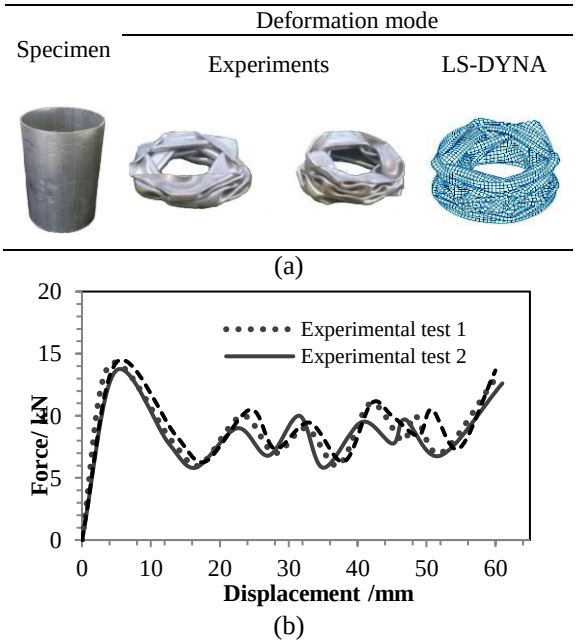

Fig. 4. (a) Deformation mode and (b) force-displacement curve.

5. Optimization by response surface methodology

The main objective of this research is to optimize the dimensions of the tapered structures depicted in Fig. 1, using the response surface (RS) methodology in parallel with the LS-DYNA

analyses. To assess the crashworthiness capacity of the structures studied in this research, two conflicting crush indicators, namely the energy absorption (*EA*) and the peak crushing force (*PCF*), are considered. The *EA* is used as a key indicator to measure the amount of energy absorbed by any structure which can be calculated using the following equation:

$$EA = \int_0^{\delta} F(x)dx \qquad (2)$$

where, *F(x)* is the variations of crushing force, and δ is the total axial displacement of the rigid-wall which is assumed 225mm in this research. Obviously, an efficient structure must have a higher amount of *EA*. On the other hand, the *PCF* is the maximum value of *F(x)* and is one of the most important crush indicators for the safety of the vehicle passengers. The more deceleration (negative acceleration at the moment of collision) increases the amount of *PCF*. This parameter is known as the negative factor in the structural design of vehicles, so is tried to be minimized. In the first step of optimization, the design points are determined by the design of experiment (DOE) techniques such as HDD (historical data design) in the Design-Expert software. The structures with dimensions of the design points are then analyzed in LS-DYNA to find the crush indicators. Next, the RS models are built using the crush indicators obtained from the finite element analyses. These models indeed state the relationship between the crush indicators and the design (geometrical) parameters. The RS models can produce an efficient prediction of the crush indicators for the given dimensions. Moreover, the RS models can be used to indicate which design parameter affects any crush indicator more [38].

Cross-sectional perimeter (denoted by P herein) of all the tapered structures at the small end is the design parameter studied in this research. It is varied between 20 mm and 320 mm to achieve the maximum *EA* and the minimum *PCF*.

Fig. 5 shows the flowchart of the implementing RS methodology for optimization problem. From the HDD method, nine design points (with different P between 20 mm and 320 mm) are selected for all the tapered structures to optimize the dimension of P (see Table 2). It is noticed that the geometry of the structures is straight for *P*=320 mm rather than tapered. In addition, a decrease (or increase) in the perimeter (*P*) increases (or decreases) the tapered angle (θ) of the structures. The FE model validated in LS-DYNA is used to analyze the collapse behavior of the tapered structures under multiple loading angles. Table 2 displays the numerical results of the EA and PCF for all these structures. Subscripts 1 to 4 for the EA and PCF correspond to the loading angles 0° to 30°, respectively.

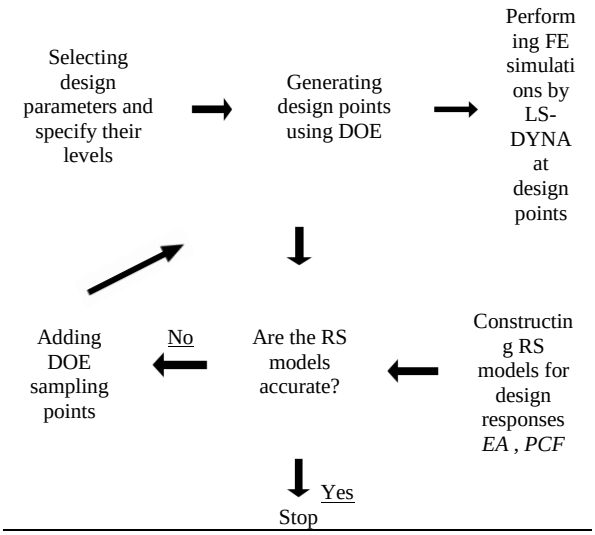

Fig. 5. Flowchart of implementing the RS methodology for optimization of the tapered structures.

Fig. 6 indicates the mutual influence of *EA* and cross-sectional perimeter *P* under multiple loading angles. From Fig. 6, by increasing P, the *EA* initially decreases sharply, then gently decreases, and finally decreases sharply again for all the structures. Generally, it can be clearly observed that the decagonal and square structures have the highest and lowest value of *EA*, respectively under multiple loading angles.

Table 2. The design points and numerical results for the tapered structures with (a) square, (b) hexagonal, (c) octagonal, (d) decagon, and (e) circular cross-sections.

(a)

			$\alpha=0^0$		$\alpha=10^0$		$\alpha=20^0$		$\alpha=30^0$	
No	*P*/*mm*	*t*/*mm*	EA_1/kJ	PCF_1/kN	EA_2/kJ	PCF_2/ kN	EA_3/kJ	PCF_3/ kN	EA_4/kJ	PCF_4/ kN
1	320	1.82	9.21	87.59	7.69	72.36	3.48	44.03	2.68	40.07
2	280	1.93	10.36	84.33	8.62	69.67	3.88	42.69	2.81	38.26
3	240	2.07	11.2	78.5	9.4	64.87	4.15	40.21	3.23	35.42
4	200	2.23	11.66	80.08	9.63	66.16	4.42	40.5	3.52	33.46
5	160	3.38	11.14	82.93	9.36	68.52	3.9	40.82	3.14	36.97
6	120	2.6	12.11	85.97	10.1	73.03	4.61	43.97	3.44	38.86
7	80	2.89	12.53	80.56	10.67	66.55	5.06	46.63	3.82	42.32
8	40	3.17	13.96	102.12	11.89	82.47	5.49	51.86	4.21	45.81
9	20	3.45	14.7	110.96	12.98	92.62	5.85	58.46	4.67	52.27

(b)

			$\alpha=0^0$		$\alpha=10^0$		$\alpha=20^0$		$\alpha=30^0$	
No	*P*/*mm*	*t*/*mm*	EA_1/kJ	PCF_1/kN	EA_2/kJ	PCF_2/ kN	EA_3/kJ	PCF_3/ kN	EA_4/kJ	PCF_4/ kN
1	320	1.74	9.75	90.65	8.44	78.30	3.90	45.89	3.21	41.98
2	280	1.87	10.83	87.71	9.22	77.53	4.08	43.81	3.57	39.15
3	240	2	11.47	85.16	10.21	72.30	4.77	40.57	3.84	36.26
4	200	2.14	12.54	76.93	10.60	67.07	5.26	42.34	4.19	37.76
5	160	2.3	12.59	81.83	11.20	71.87	4.57	38.31	3.92	33.83
6	120	2.51	12.64	83.88	10.34	72.93	4.99	43.35	4.18	38.67
7	80	2.76	13.01	93.78	11.60	83.87	5.55	50.29	4.44	43.73
8	40	3.06	14.45	104.27	12.89	91.49	6.12	53.38	4.96	48.74
9	20	3.38	15.51	115.09	13.77	101.94	6.59	62.40	5.19	55.51

(c)

			$\alpha=0^0$		$\alpha=10^0$		$\alpha=20^0$		$\alpha=30^0$	
No	*P*/*mm*	*t*/*mm*	EA_1/kJ	PCF_1/kN	EA_2/kJ	PCF_2/ kN	EA_3/kJ	PCF_3/ kN	EA_4/kJ	PCF_4/ kN
1	320	1.69	10.04	92.09	8.78	78.87	4.06	49.51	3.61	44.52
2	280	1.82	10.69	89.30	9.68	75.74	4.40	49.02	3.94	44.08
3	240	1.95	11.79	84.11	11.10	68.52	4.83	45.71	4.19	41.11
4	200	2.19	11.45	84.71	10.62	71.14	5.32	42.41	4.57	38.13
5	160	2.26	13.16	85.39	11.44	73.24	5.35	44.36	4.67	39.89
6	120	2.46	13.43	85.69	11.74	76.39	4.99	45.57	4.33	40.98
7	80	2.72	13.75	95.44	12.29	84.15	5.66	53.03	4.94	47.68
8	40	3.01	14.87	104.41	13.26	93.60	6.40	58.39	5.37	52.50
9	20	3.29	15.66	116.72	14.14	105.91	6.72	64.46	5.77	57.96

(d)

			$\alpha=0^0$		$\alpha=10^0$		$\alpha=20^0$		$\alpha=30^0$	
No	*P*/*mm*	*t*/*mm*	EA_1/kJ	PCF_1/kN	EA_2/kJ	PCF_2/ kN	EA_3/kJ	PCF_3/ kN	EA_4/kJ	PCF_4/ kN
1	320	1.76	10.44	95.09	8.98	79.10	4.23	50.27	3.73	46.48
2	280	1.88	11.52	94.15	9.69	78.31	4.44	46.87	4.18	45.06
3	240	2.01	12.33	88.80	10.53	74.03	4.89	43.41	4.32	42.72
4	200	2.17	13.44	86.46	11.25	71.65	5.30	45.22	4.60	39.59
5	160	2.32	13.65	8320	11.65	69.77	6.15	43.51	5.33	36.63
6	120	2.52	13.22	86.53	11.27	75.35	5.73	45.30	4.93	40.93
7	80	2.79	14.18	98.85	12.20	83.84	5.90	54.36	5.28	47.99
8	40	3.1	15.76	114.23	13.55	94.48	6.59	59.36	5.63	53.36
9	20	3.4	16.58	120.80	14.68	104.34	7.10	66.46	6.13	60.43

(e)

			$\alpha=0^0$		$\alpha=10^0$		$\alpha=20^0$		$\alpha=30^0$	
No	*P*/*mm*	*t*/*mm*	EA_1/kJ	PCF_1/kN	EA_2/kJ	PCF_2/ kN	EA_3/kJ	PCF_3/ kN	EA_4/kJ	PCF_4/ kN
1	320	1.71	9.72	92.41	8.10	73.92	3.57	45.37	3.06	40.58
2	280	1.83	10.97	90.78	8.76	70.58	4.15	43.57	3.38	37.84
3	240	1.96	11.75	84.25	9.89	65.36	4.31	40.44	3.62	35.04
4	200	2.11	12.74	85.27	10.92	68.21	4.82	40.93	3.92	36.50
5	160	2.27	12.37	83.53	9.48	61.73	4.58	38.05	3.73	32.70
6	120	2.48	12.31	87.31	10.36	69.84	4.66	42.92	3.79	37.37
7	80	2.73	13.43	98.73	11.52	81.02	5.34	48.41	4.36	42.26
8	40	3.02	15.05	110.05	12.71	86.01	5.81	53.84	4.87	47.11
9	20	3.31	15.74	120.56	13.82	100.53	6.18	60.93	5.09	53.65

On the other hand, based on Fig. 7, by increasing *P*, the *PCF* initially decreases nonlinearly and then increases for all the structures under multiple loading angles. Hence, a minimum value for the *PCF* is observed.

The multi-objective optimization problem can be solved by two methods. The first one is to study all the crush indicators independently and to search for a set of optimal solutions (known as the Pareto optimal solution) [38]. The second method, called desirability approach, incorporates different objective functions into a single objective function. Hence, it results in a single solution for the optimization problem [38-41]. The second technique is used in the present task. In a single objective function, called desirability, the predicted response is transformed into a dimensionless value, called desirability, ranging from 0 to 1.

If the desirability value is 1, it corresponds to the ideal solution, while the desirability value of zero represents the worst solution. It is evident that the more closeness to 1, the better solution is achieved.

In the process of optimization, *EA* is used as a useful and positive criterion, and *PCF* is used as a negative criterion. The weight selection for input factors has a great impact on the optimum design of structures. This is one of the most important parameters in multi-objective optimization methods. Thus, the weight of *EA* and PCF are taken 0.65 and 0.35, respectively. The numerical results (EA_{1-4} and PCF_{1-4}) presented in Table 2 are incorporated into Design-Expert software, as the input data, and then analyzed to obtain the optimal *P*. Fig. 8 displays variations of the desirability as a function of the perimeter *P*. The optimized structures are selected by this fact to have higher EA and lower PCF. The optimal points for the tapered structures marked by D_{1-5} in Fig. 8 are presented in Table 3. The corresponding tapered

angle θ and crush indicators for the optimal design of the tapered structures have been also given in Table 3. It is evident from Table 3 that the tapered angle θ increases (or the perimeter P decreases) as the side number of the cross-section enhances.

6. Collapse behaviors of the tapered structures

The optimal tapered structures, having the optimum dimensions shown in Table 3, are analyzed in LS-DYNA. The deformation modes together with the force-displacement curves are given in Figs. 9 and 10, respectively. As is seen in Fig. 9, all the tapered structures show diamond progressive folding mode under axial loading. The mixed diamond and local bending mode are observed for the loading angle 10°. While all the structures collapse in the global bending mode for over the loading angle 10° namely 20° and 30°. It is well known that the progressive folding mode and the global bending mode provide the most suitable and unsuitable crushing deformation modes, respectively.

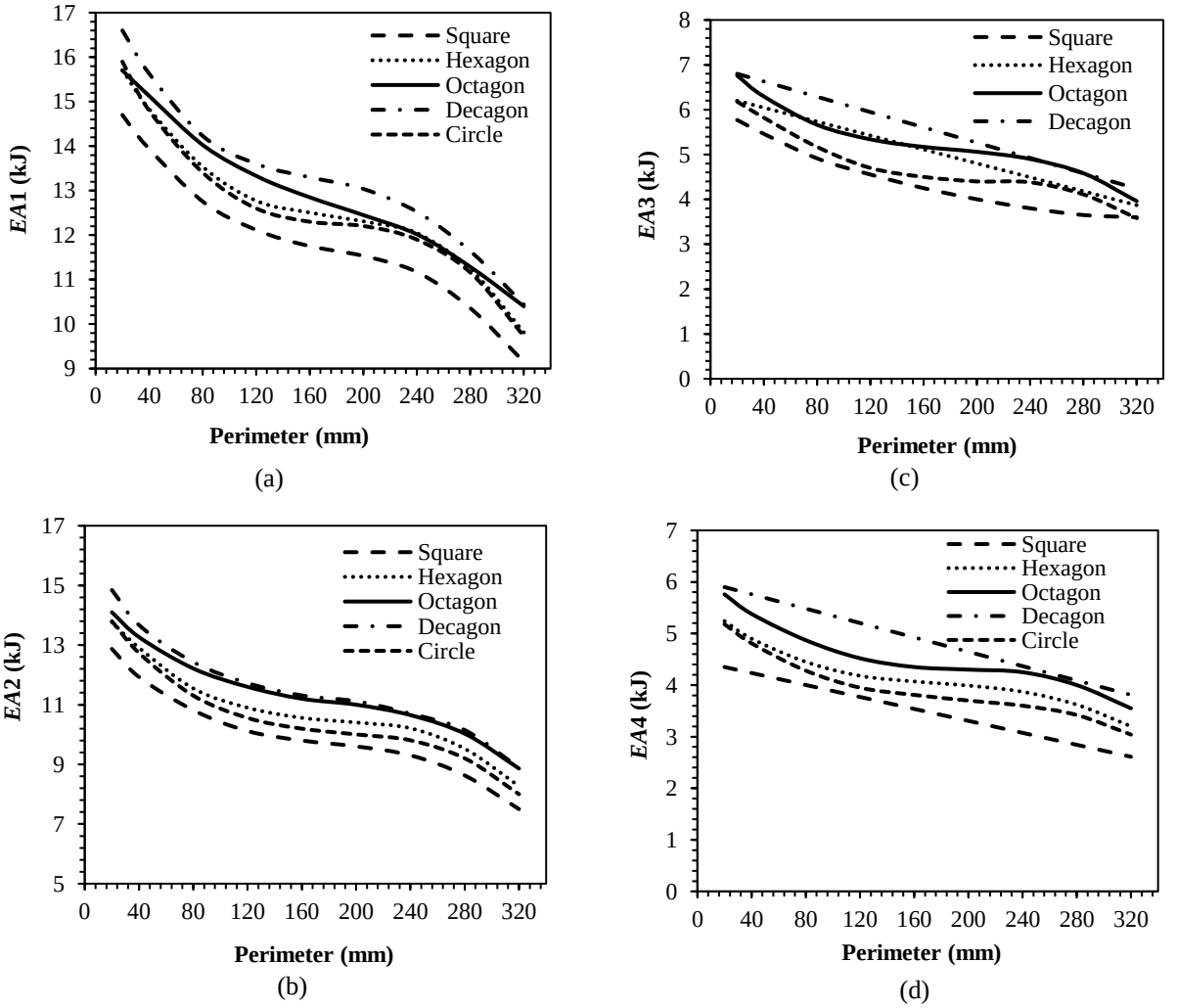

Fig. 6. Variations of EA vs P for all the studied tapered structures under different loading angles of (a) α=0˚, (b) α=10˚, (c) α=20˚, and (d) α=30˚

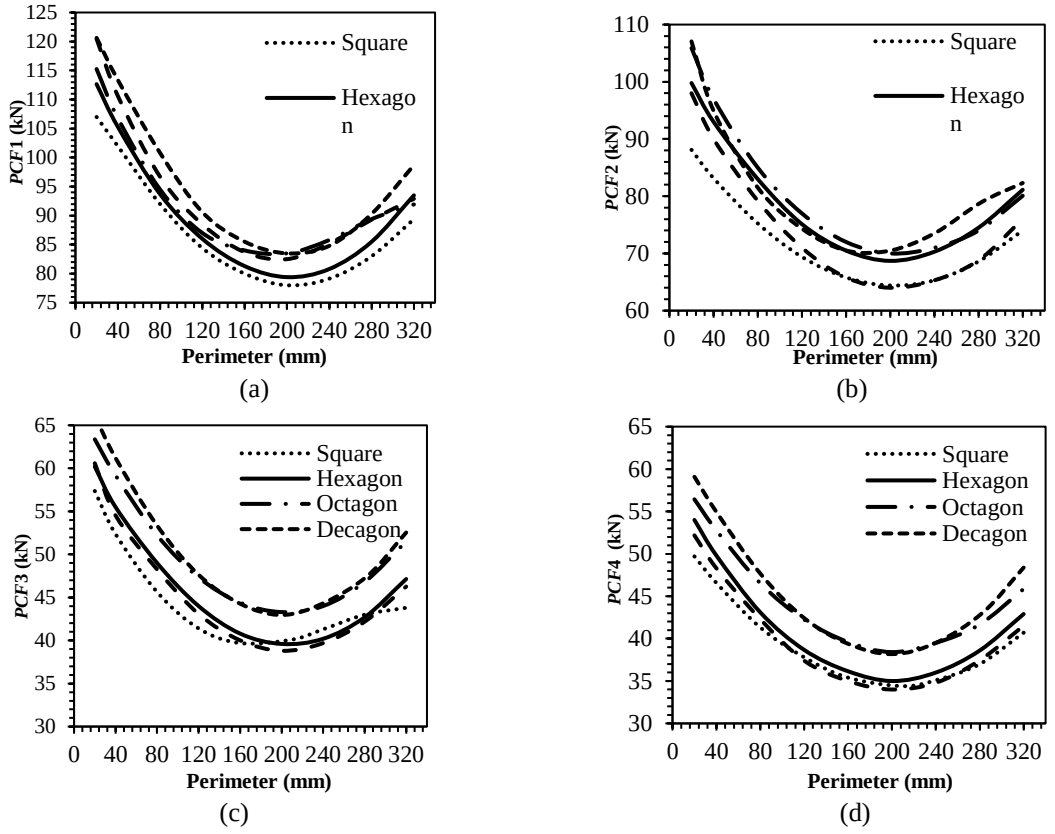

Fig. 7. Variations of PCF vs P for all the studied tapered structures under different loading angles of (a) α=0˚, (b) α=10˚, (c) α=20˚, and (d) α=30˚.

However, oblique loading is inevitable in the real car collision, which results in undesirable deformations (or global bending) in the structures.

From the force-displacement curves displayed in Fig.10, it is evident that all the structures have the same manner. In other words, for the axial loading and small oblique loading of 10°, the force initially increases to reach its peak value, then decreases and follows in a number of oscillations. It is well known that each force fluctuation represents forming one wrinkle in the structures. When the structures experience the oblique crush (20° and 30°), the force gradually enhances (which is prominent by increasing the loading angle) to reach its peak value, and afterward decreases gently due to global bending mode occurs in the structures. It is worth mentioning that by comparing with the straight structures [20], the tapered structures are more preferable as they consist of stable force-displacement curves and lower peak force.

Table 3. The perimeter P and the corresponding tapered angle θ and crush indicators for the optimal design of the tapered structures.

	Indicators	***D1***	***D2***	***D3***	***D4***	***D5***
	P/mm	179.3	173.9	157.7	145.1	178.5
	a/mm	44.82	28.98	19.71	14.51	56.84
	Θ/^{0}	3.25	4.3	4.5	4.8	4.15
α =0^0	EA_1/kJ	11.56	12.41	12.87	13.38	12.32
	PCF_1/kN	78.78	81.36	82.68	84.81	83.76
α=10^0	EA_2/kJ	9.83	10.61	11.09	11.34	10.12
	PCF_2/kN	65.46	70.11	72.05	71.23	66.64
α=20^0	EA_3/kJ	4.46	5.04	5.16	5.63	4.63
	PCF_3/kN	40.37	41.25	43.38	44.45	39.44
α=30^0	EA_4/kJ	3.45	4.05	4.49	5.02	3.77
	PCF_4/kN	35.35	35.76	37.91	39.86	34.28

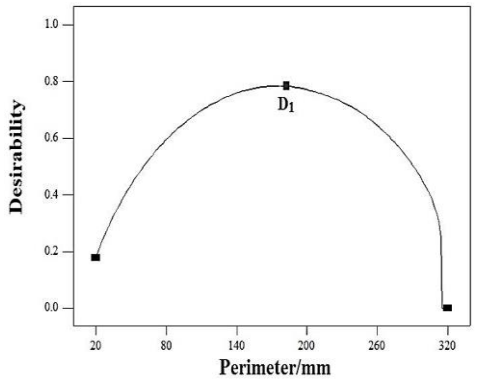

(a)

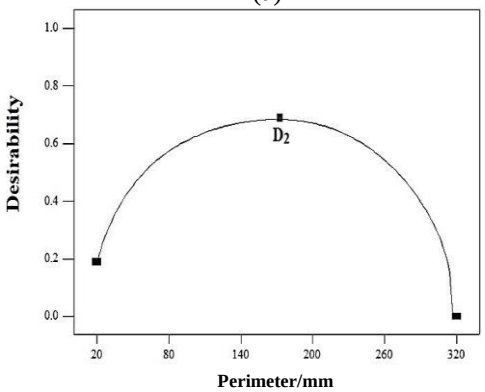

(b)

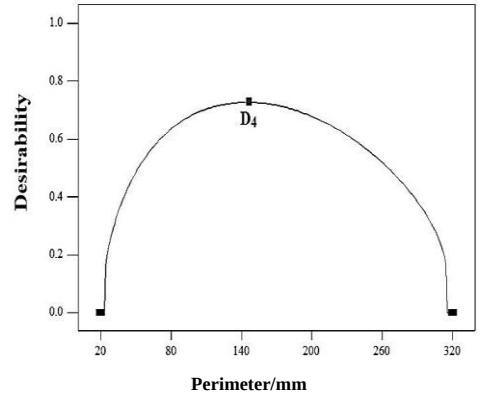

(c)

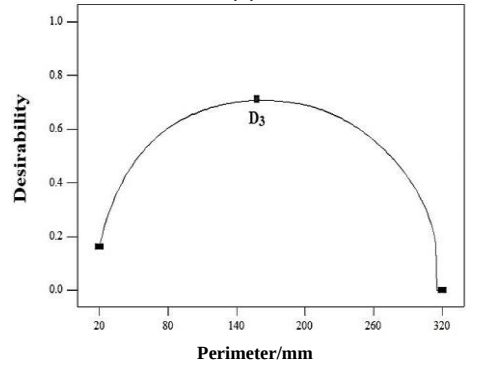

(d)

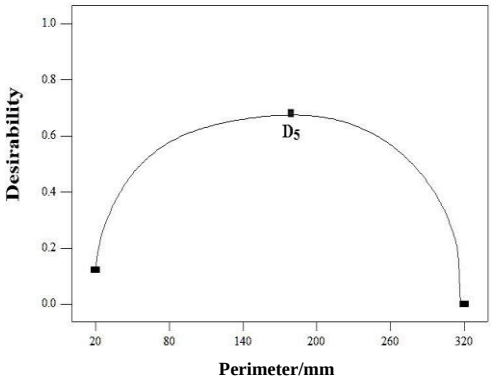

(e)

Fig. 8. Desirability vs the perimeter for the tapered structures with cross-sections of (a) square, (b) hexagonal, (c) octagonal, (d) decagon, and (e) circular.

Section	$\alpha=0^0$	$\alpha=10^0$	$\alpha=20^0$	$\alpha=30^0$
Square				
Hexagon				
Octagon				
Decagon				
Circle				

Fig. 9. Deformation modes of the optimal structures under multiple loading angles.

7. Multi-criteria decision-making methods (TOPSIS)

In order to select the structure with the best performance in terms of energy absorption capacity for reducing the damage to vehicle parts and passengers, TOPSIS method is adopted. This method is widely used to solve the problems related to the selection of the best

design regarding different criteria and indicators [39, 42, 43]. Steps of applying this method are presented below:
The first step: Forming the decision matrix as below;

$$A_{ij} = \begin{bmatrix} a_{11} & a_{12} & \dots & a_{1n} \\ a_{21} & a_{22} & \dots & a_{2n} \\ \dots & \dots & \dots & \dots \\ a_{m1} & a_{m2} & \dots & a_{mn} \end{bmatrix} \quad (3)$$

m criteria as matrix row and n options as matrix column.

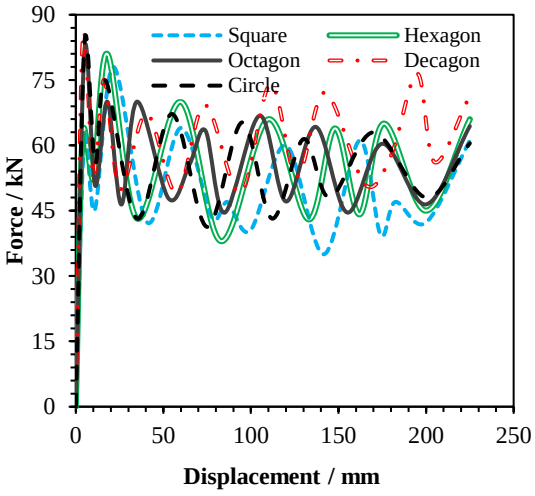

(a)

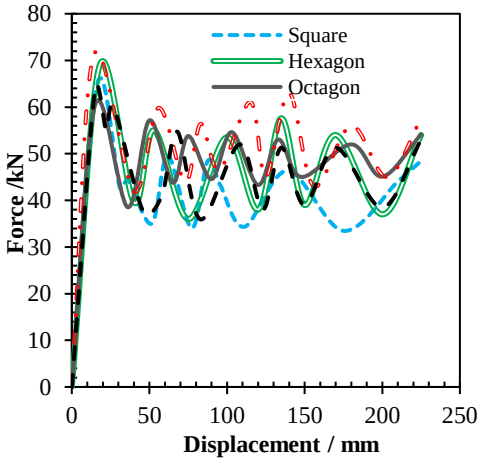

(b)

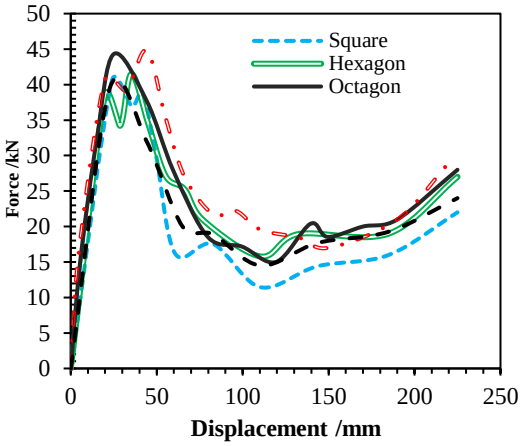

(c)

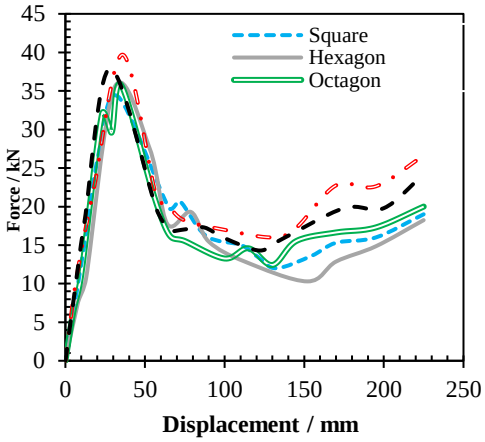

(d)

Fig. 10. Force-displacement curves for the optimal tapered structures under loading angles of (a) α=0˚, (b) α=10˚, (c) α=20˚, and (d) α=30˚.

The second step: Normalizing the decision matrix:

$$r_{ij} = \frac{a_{ij}}{\sqrt{\sum_{K=1}^{m} a^2_{ij}}} \quad (4)$$

The third step: In this step, the weight of each criterion is applied such that more important criterion is given higher weight value. Indeed, matrix V_{ij} is obtained by multiplying the standard values of each criterion by the relevant weights.

$$V_{ij} = \begin{bmatrix} w_1 r_{11} & w_2 r_{12} & \dots & w_n r_{1n} \\ w_1 r_{21} & w_2 r_{22} & \dots & w_n r_{2n} \\ \dots & \dots & \dots & \dots \\ w_1 r_{m1} & w_2 r_{m2} & \dots & w_n r_{mn} \end{bmatrix} \quad (5)$$

The fourth step: Determining the positive ideal solution (A^+) and the negative ideal solution (A^-):

$$A^+ = \left\{ (\max v_{ij} \,\middle|\, j \in J), (\min v_{ij} \,\middle|\, j \in J') \right\}$$

$$A^+ = \left\{ v^+{}_1, v^+{}_2, \dots v^+{}_n \right\}$$

$$A^- = \left\{ (\min v_{ij} \,\middle|\, j \in J), (\max v_{ij} \,\middle|\, j \in J') \right\}$$

$$A^- = \left\{ v^-{}_1, v^-{}_2, \dots v^-{}_n \right\} \quad (6)$$

The fifth step: Obtaining the distance between the positive ideal (S_i^+) or the negative ideal (S_i^-) and each option:

$$S_i^+ = \sqrt{\sum_{j=1}^{n} (v_{ij} - v_j^+)^2} \quad (7)$$

$$S_i^- = \sqrt{\sum_{j=1}^{n} (v_{ij} - v_j^-)^2}$$

The sixth step: Determining the proximity coefficient of each option (C_i^+):

$$C_i^+ = \frac{S_i^-}{S_i^+ + S_i^-} \quad (8)$$

The option with the highest value of C_i^+ is selected as the best energy absorber. The best energy absorber is introduced by implementing this method on the results of the optimal structures. Table 4 presents the decision matrix in which there exist 8 criteria and 5 options. The objective of TOPSIS is to rank the options in order of crashworthiness capacity considering two conflicting criteria of EA and PCF at four loading angles (totally 8 criteria). Tables 5 and 6 show the normalized and weighted normalized decision matrix calculated by Eqs. 4 and 5, respectively. Because the EA (as a useful index) is more important than PCF (as a negative index), so their weights are assumed 0.65 and 0.35, respectively. Table 7 shows the distance matrix of each option with the positive ideal (S_i^+) and negative ideal (S_i^-) solutions. The results of TOPSIS calculations are finally given in Table 8 from which ranking of the tapered structures is found as decagonal, octagonal, hexagonal, circular, and square. As a result, the decagonal tapered structure is introduced as the best energy absorber due to having more corners and sides. It is also worth noting that the reinforcing plates used in the considered structures offered additional corners, compared with the single-cell structures without these plates, which increase the crashworthiness capacity of the structures.

Table 4. Decision matrix

Loading angle		Square	Hexagon	Octagon	Decagon	Circular
$\alpha=0^0$	EA_1	11.56	12.41	12.87	13.38	12.32
	PCF_1	78.78	81.36	82.68	84.81	83.76
$\alpha=10^0$	EA_2	9.83	10.61	11.09	11.34	10.12
	PCF_2	65.46	70.11	72.05	71.23	66.64
$\alpha=20^0$	EA_3	4.46	5.04	5.16	5.63	4.63
	PCF_3	40.37	41.25	43.38	44.45	39.44
$\alpha=30^0$	EA_4	3.45	4.05	4.49	5.02	3.77
	PCF_4	35.35	35.76	37.91	39.86	34.28

Table 5. Normalized decision matrix r_{ij}

Loading angle		Square	Hexagon	Octagon	Decagon	Circular
$\alpha=0^0$	EA_1	0.412835	0.44319	0.459618	0.477831	0.439976
	PCF_1	0.428062	0.442081	0.449254	0.460827	0.455122
$\alpha=10^0$	EA_2	0.414212	0.447079	0.467305	0.477839	0.426432
	PCF_2	0.42337	0.453445	0.465992	0.460689	0.431002
	EA_3	0.398831	0.450697	0.461427	0.503457	0.414033

α=20^0	PCF_3	0.4317 11	0.4411 21	0.463899	0.475342	0.421765
	EA_4	0.3680 26	0.4320 3	0.478967	0.535504	0.402161
α=30^0	PCF_4	0.4309 21	0.4359 19	0.462128	0.485899	0.417878

Table 6. Weighted normalized decision matrix

Loading angle		Square	Hexagon	Octagon	Decagon	Circular
α=0^0	EA_1	0.26 8343	0.28 8074	0.29 8752	0.31 059	0.28 5984
	PCF_1	0.14 9822	0.15 4728	0.15 7239	0.16 129	0.15 9293
α=10^0	EA_2	0.26 9238	0.29 0601	0.30 3748	0.31 0596	0.27 7181
	PCF_2	0.14 8181	0.15 8706	0.16 3097	0.16 1241	0.15 0851
α=20^0	EA_3	0.25 9241	0.29 2953	0.29 9928	0.32 7247	0.26 9121
	PCF_3	0.15 1099	0.15 4392	0.16 2365	0.16 6371	0.14 7618
α=30^0	EA_4	0.23 9217	0.28 0821	0.31 1328	0.34 8078	0.26 1405
	PCF_4	0.15 0822	0.15 2572	0.16 1745	0.17 0065	0.14 6257

Table 7. Distance of each option with (a) the positive ideal S_i^+ and (b) negative ideal S_i^-.

(a)

Loading angle		Square	Hexagon	Octagon	Decagon	Circular
α=0^0	EA_1	0.00 1785	0.00 0507	0.00 014	7.97 E-14	0.00 0605
	PCF_1	0.00 0132	4.31 E-05	1.64 E-05	2.17 E-13	3.99 E-06
α=10^0	EA_2	0.00 1711	0.00 0451	4.69 E-05	1.24 E-13	0.00 1117
	PCF_2	0.00 0223	1.93 E-05	3.52 E-14	3.44 E-06	0.00 0151
α=20^0	EA_3	0.00 4624	0.00 1176	0.00 0746	4.68 E-11	0.00 3378
	PCF_3	0.00 0233	0.00 0143	1.62 E-05	2.13 E-13	0.00 0352
α=30^0	EA_4	0.01 1851	0.00 4524	0.00 1351	2.11 E-13	0.00 7512
	PCF_4	0.00 0371	0.00 0306	6.92 E-05	2.27 E-13	0.00 0567

(b)

Loading angle		Square	Hexagon	Octagon	Decagon	Circular
α=0^0	EA_1	1.804 E-13	0.00 0389	0.00 092	0.00 178	0.00 0311
	PCF_1	2.861 E-14	2.41 E-05	5.5E -05	0.00 013	8.97 E-05
α=10^0	EA_2	1.067 E-13	0.00 0456	0.00 119	0.00 171	6.31 E-05
	PCF_2	1.414 E-13	0.00 0111	0.00 022	0.00 017	7.13 E-06
α=20^0	EA_3	1.596 E-09	0.00 1139	0.00 165	0.00 463	9.84 E-05
	PCF_3	1.224 E-05	4.61 E-05	0.00 021	0.00 035	3.2E-10
α=30^0	EA_4	1.319 E-13	0.00 1731	0.00 52	0.01 185	0.00 0492
	PCF_4	2.084 E-05	3.99 E-05	0.00 024	0.00 056	3.88 E-14

Table 8. The results of ranking obtained from the TOPSIS calculations.

	Square	Hexagon	Octagon	Decagon	Circular
S^+	0.144664	0.084368	0.048839	0.001856	0.116981
S^-	0.005752	0.062742	0.098539	0.145593	0.032586
C^+	0.038241	0.426499	0.668615	0.987412	0.217871
Ranking	5	3	2	1	4
					

7. Conclusions

In this article, energy absorption performance of multi-cell tapered structures with square, hexagonal, octagonal, decagon and circular cross sections under axial and oblique dynamic loading is numerically evaluated. The important results are drawn as follows:

- The experimentally validated finite element model in LS-DYNA is used to calculate the crush indicators including peak crushing force (*PCF*) and energy absorption (*EA*) for the tapered structures.
- For the axial loading and small oblique loading of 10°, the force initially increases

to reach its peak value, then decreases and follows in a number of oscillations. While, for the larger oblique crushes (20° and 30°), the force gradually increases to reach its peak value, and then reduces gently.

- For the axial impact loading, the structures show diamond progressive folding mode, and for the impact angle of 10°, they show a mixed diamond and bending modes. Whereas, for the larger oblique loads (i.e. 20° and 30°), they show a pure global bending mode.
- The perimeter (*i.e.* tapered angle) of the structures is optimized using the RS methodology and desirability approach. The results reveal that the optimal tapered angle increases as the number of cross-section sides enhances.
- The TOPSIS method is implemented on the results of the optimal tapered structures, and the structure with the decagonal cross-section is found as the best and suitable energy absorber.

References

[1] A. Morris, C. Brace, S. Reed, H. Fagerlind, et al., "The development of a European fatal accident database", *Int. J of Crashworthiness*, Vol. 15, No. 2, pp. 201-209, (2010).

[2] R. Welsha, A. Morris, A. Hassan, J. Charlton, "Crash characteristics and injury outcomes for older passenger car occupants", *Transportation Research Part F: Traffic Psychology and Behaviour*, Vol. 9, No. 5, pp. 322-334, (2006).

[3] S. Reed, A. Morris, "Characteristics of fatal single-vehicle crashes in Europe", *Int J of Crashworthiness*, Vol. 17, No. 6, pp. 655-664, (2012).

[4] J. M. Alexander, "An approximate analysis of the collapse of thin cylindrical shells under axial loading" , *Quarterly J. of Mech. Applied Math.*, Vol. 13, No.1, pp. 10-5, (1960).

[5] W. Abramowicz and N. Jones, "Dynamic progressive buckling of circular and square tubes", *Int. J. Impact. En.*, Vol.4, No. 1, pp. 243-270, (1986).

[6] S. R. Guillow, G. X. Lu, R.H. Grzebieta, "Quasi-static axial compression of thin-walled circular aluminum tubes", *Int. J. Mech. Sci.*, Vol. 43, No. 9, pp. 2103-2123, (2001).

[7] A. Niknejad and M. Moeinifard, "Theoretical and experimental studies of the external inversion process in the circular metal tubes", *Materials & Design*, Vol. 40, No. 1, pp. 324-330, (2012).

[8] A. G. Mamalis, D. E. Manolakos, A. K. Baldoukas, "Energy dissipation and associated failure modes when axially loading polygonal thin-walled cylinders", *Thin-Walled Structures*, Vol. 12, No. 1, pp. 17-34, (1991).

[9] W. Abramowicz, N. Jones, "Dynamic axial crushing of square tubes", *Int J Impact Eng*, Vol. 2, No. 2, pp. 179-208, (1984).

[10] A. G. Hanssen, M. Langseth, O. S. Hopperstad, "Static and dynamic crushing of circular aluminium extrusions with aluminium foam filler", *Int J Impact Eng*, Vol. 24, No. 5, pp. 475-507, (2000).

[11] H. Mozafari, S. Khatemi, H. Molatefi, "Finite element analysis of foam-filled honeycomb structures under impact loading and crashworthiness design*", Int J crashworthiness*, Vol. 21, No. 2, pp. 148-160, (2016).

[12] H. Mozafari, S. Khatami, H. Molatefi, "Out of plane crushing and local stiffness determination of proposed foam filled sandwich panel for Korean Tilting Train Express Numerical study", *Material and Design*, Vol. 66, No. 2, pp. 400-411, (2015).

[13] M. Seitzberger, F. G. Rammerstorfer, R. Gradinger, "Experimental studies on the quasi-static axial crushing of steel columns filled with aluminum foam" *Int J Solids Struct*, Vol. 37, No. 30, pp. 4125-4147, (2000).

[14] L. Aktay, A. Toksoy, M. Guden, "Quasi-static axial crushing of extruded polystyrene foam-filled thin-walled

aluminum tubes: Experimental and numerical analysis", *Mat and Des*, Vol. 7, No. 5, pp. 556-565, (2006).

[15] A. Ghamarian, H. R. Zarei, M. T. Abadi, "Experimental and numerical crashworthi- ness investigation of empty and foam-filled end-capped tapered tubes", *Thin-Walled Struct*, Vol. 49, No. 10, pp. 1312-9 (2011)

[16] W. G. Chen and T Wierzbicki, "Relative merits of single-cell multi-cell and foam-filled thin-walled structures in energy absorption", *Thin-Walled Struct*, Vol. 39, No. 4, pp. 287-306, (2001).

[17] W. Abramowicz and N. Jones, "Dynamic axial crushing of square tubes", *Int J Impact Eng*, Vol. 2, No. 2, pp. 179-208, (1984).

[18] W. Abramowicz and N. Jones, "Dynamic progressive buckling of circular and square tubes.", *Int J Impact Eng*, Vol. 4, No. 4, pp. 243-70, (1986).

[19] M. Langseth, O. S. and Hopperstad, "Static and dynamic axial crushing of square thin- walled aluminium extrusions*", Int. J. Mech. Sci.*, Vol. 18, No. 7-8, pp. 946 – 968, (1996).

[20] P. Hosseini-Tehrani and S Pirmohammad, "Collapse study of thin-walled polygonal section columns subjected to oblique loads", *Proc Inst Mech Eng: Part D: J. Automobile Eng.* , Vol. 221, No. 7, pp. 801- 810, (2007).

[21] A. Eyvazian, "Mathematical Model for Thin-walled Corrugated Tube under Axial Compression, MATEC Web of Conferences: International Conference on Mechanical Engineering and Electrical Systems (ICMES)", 40:02010, 29 January (2016).

[22] A. Eyvazian, M. Habibi, A. M Hamouda, "Axial crushing behavior and energy absorption efficiency of corrugated tubes", *Mat and Des*, Vol. 54, No. 1, pp. 1028-1038, (2014).

[23] A. Eyvazian, "Experimental study of corrugated tubes under lateral loading", *Proc. Inst. Mech. Eng. Part L: J of Mat: Des and App*, Vol. 226, No. 2, (2012).

[24] H. S. Kim, "New extruded multi-cell aluminum profile for maximum crash energy absorption and weight efficiency", *Thin-Walled Struct*, Vol. 40, No. 4, pp. 311-327, (2002).

[25] X. Zhang and G. Cheng, "A comparative study of energy absorption characteristics of foam-filled and multi-cell square columns*", Int J of Impact Eng*, Vol. 34, No. 7-8, pp. 1739-1752, (2007).

[26] N. Qiu, Y. Gao, J. Fang, "Crashworthiness analysis and design of multi-cell hexagonal columns under multiple loading cases*", Finite Elem Anal Des*, Vol. 104, No. 1, pp. 89-101, (2015).

[27] S. Pirmohammad and S. Esmaeili Marzdashti, "Crushing behavior of new designed multi-cell members subjected to axial and oblique quasi-static loads", *Thin-Walled Struct*, Vol. 108, No. 11, pp. 291-304, (2016).

[28] S. Pirmohammad and S. Esmaeili Marzdashti, "Crashworthiness optimization of combined straight-tapered tubes using genetic algorithm and neural networks", *Thin-Walled Struct.*, Vol. 127, No. 1, pp. 318-332, (2018).

[29] Q. Chang, Y. Shu, D. Fangliang, "Crushing analysis and multiobjective crashworthiness optimization of tapered square tubes under oblique impact loading". *Thin-Walled Struct*, Vol. 59, No. 10, pp. 103-119, (2012).

[30] P. Hosseini-Tehrani, S. Pirmohammad, M. Golmohammadi, "Study on the collapse of tapered tubes subjected to oblique loads", *Proc Inst Mech Eng: Part D. J. Automobile Eng.*, Vol. 222, No. 11, pp. 2025-2039, (2008).

[31] Y. Hanfeng, W. Guilin, F. Hongbing, "Multiobjective crashworthiness optimization design of functionally graded foam-filled tapered tube based on dynamic ensemble metamodel", *Mat and Des*, Vol. 55, No. 1, pp. 747-757, (2014).

[32] Z. Ahmad, D. P. Thambiratnam, "Crushing response of foam-filled conical tubes under quasi-static axial loading".

Mater Des, Vol. 30, No. 7, pp. 2393-2403, (2009).

[33] Z. Ahmad, D. P. Thambiratnam, "Dynamic computer simulation and energy absorption of foam-filled conical tubes under axial impact loading". *Computers and Structures*, Vol. 87, No. 3-4, pp. 186-197, (2009).

[34] Z. Ahmad, D. P. Thambiratnam, A. C. Tan, "Dynamic energy absorption characteristics of foam-filled conical tubes under oblique impact loading", *Int J Impact Eng*, Vol. 37, No. 5, pp. 475-488, (2010).

[35] A. Ghamarian, H. R. Zarei, M. Abadi, "Experimental and numerical crashworthiness investigation of empty and foam-filled end-capped conical tubes", *Thin-Walled Struct*, Vol. 49, No. 10, pp. 1312-1319, (2011).

[36] M. Langseth, O. S Hopperstad, "Static and dynamic axial crushing of square thin-walled aluminium extrusions", *Int J of Impact Eng*, Vol. 18, No. 7-8, pp. 949-968, (1996).

[37] X. Zhang, H. Zhang, "Energy absorption of multi-cells tube columns under axial compression", *Thin-Walled Struct*, Vol. 68, No. 1, pp. 156-163, (2013).

[38] A. Baroutaji, M. D. Gilchrist, D. Smyth, "Crush analysis and multi-objective optimization design for circular tube under quasi-static lateral loading", *Thin-Walled Struct*, Vol. 86, No. 1, pp. 121-131, (2015).

[39] A. Baroutaji, E. Morris, A. G. Olabi, "Quasi-static response and multi-objective crashworthiness optimization of oblong tube under lateral loading", *Thin Walled Struct*, Vol. 82, No. 1, pp. 262-277, (2014).

[40] S. Hou, "Crashworthiness design for foam filled thin-wall struct", *Mater Des*, Vol. 30, No. 6, pp. 2024-2032, (2009).

[41] S. Saleh-ghaffari, M. Rais-Rohani, A. Najafi, "Analysis and optimiza- tion of externally stiffened crush tubes", *Thin Walled Struct*, Vol. 49, No. 3, pp. 397-408, (2011).

[42] A. Khalkhali, "Best compromising crashworthiness design of automotive S-rail using TOPSIS and modified NSGA-II", *Central South University*, Vol. 22, No. 1, pp. 121-133, (2015).

[43] A. Malek and B. Nia, "Fundamentals of Design-Expert software", 2nd EddditionTehran: pp. 93-110, (2009).

How to cite this paper:

S. Pirmohammad, S. Esmaeili-Marzdashti, A. Eyvazian, " Crashworthiness design of multi-cell tapered tubes using response surface methodology" *Journal of Computational and Applied Research in Mechanical Engineering*, Vol. 9, No. 1, pp. 57-72, (2019).

DOI: 10.22061/jcarme.2018.2825.1292

URL: http://jcarme.sru.ac.ir/?_action=showPDF&article=908